Original Article

MOLECULAR METABOLISM

Endothelial BBSome is essential for vascular, metabolic, and retinal functions

Jingwei Jiang [1], John J. Reho [1], Sajag Bhattarai [2], Ioana Cherascu [2], Adam Hedberg-Buenz [3], Kacie J. Meyer [3], Fariba Tayyari [4,5], Adam J. Rauckhorst [3], Deng Fu Guo [1], Donald A. Morgan [1], Eric B. Taylor [3,4,6], Michael G. Anderson [3,6], Arlene V. Drack [2], Kamal Rahmouni [1,5,6,7,8,*]

ABSTRACT

Objectives: Endothelial cells that line the entire vascular system play a pivotal role in the control of various physiological processes, including metabolism. Additionally, endothelial dysfunction is associated with many pathological conditions, including obesity. Here, we assessed the role of the BBSome, a protein complex composed of eight Bardet-Biedl syndrome (BBS) proteins in endothelial cells.

Methods: We studied the effects of BBSome disruption in endothelial cells on vascular function, body weight, glucose homeostasis, and the liver and retina. For this, we generated mice with selective BBSome disruption in endothelial cells through *Bbs1* gene deletion.

Results: We found that endothelial cell—specific BBSome disruption causes endothelial dysfunction, as indicated by the impaired acetylcholine-induced vasorelaxation in both the aorta and mesenteric artery. This was associated with an increase in the contractile response to thromboxane A2 receptor agonist (U46619) in the mesenteric artery. Mechanistically, we demonstrated that mice lacking the *Bbs1* gene in endothelial cells show elevated vascular angiotensinogen gene expression, implicating renin-angiotensin system activation in the vascular changes evoked by endothelial BBSome deficiency. Strikingly, our data indicate that endothelial BBSome deficiency increases body weight and fat mass and causes hepatosteatosis along with alterations in hepatic expression of lipid metabolism—related genes and metabolomics profile. In addition, electroretinogram and optical coherence tomography analyses revealed functional and structural abnormalities in the retina, evoked by absence of the endothelial BBSome.

Conclusions: Our findings demonstrate that the BBSome in endothelial cells is required for the regulation of vascular function, adiposity, hepatic lipid metabolism, and retinal function.

Keywords BBSome; Endothelial function; Body weight; Liver steatosis; Retina

1. INTRODUCTION

The endothelium lining the circulatory system not only provides a structural barrier between circulation and surrounding tissue, but also plays an essential role in the control of several physiological functions through its ability to respond to the organism's biological needs [1]. Endothelial cells are best known for their contribution to the control of blood pressure and blood flow through the release of vasoactive factors such as nitric oxide (NO), endothelin-1, and angiotensin II [2]. Endothelial cells also act as metabolic gatekeepers in key metabolic organs such as the liver and adipose tissue by mediating the delivery and storage of dietary lipids, which are critical for cardiometabolic health and disease [3,4]. In the eye, in addition to regulating vascular tone and ensuring the supply of oxygen and other nutrients meets the demand of a metabolically active tissue, endothelial cells contribute to many other functions, including acting as a blood—retina barrier that prevents circulating toxins, microorganisms, and pro-inflammatory cells from reaching the retina [5,6].

Growing evidence implicates the BBSome in the regulation of various physiological, pathological, and cellular processes, including gene expression and the trafficking of receptors to cilia and plasma membranes [7—9]. The BBSome is a protein complex composed of eight Bardet-Biedl syndrome (BBS) proteins (BBS1, 2, 4, 5, 7, 8, 9, and 18) [9—11]. The assembly of the BBSome depends on another protein complex that contains 3 BBS proteins (BBS6, 10, and 12) [12]. BBS3 is critical in the recruitment of the BBSome to the cell membrane [9]. In contrast, BBS17 controls the trafficking of the BBSome in cilia [13]. Patients and animals lacking functional BBSome and related proteins display several clinical features, including obesity, diabetes mellitus, and retinal degeneration [14,15].

The BBSome is present in the vasculature, including endothelial and smooth muscle cells [16]. Recently, we showed that smooth muscle—

[1]Department of Neuroscience and Pharmacology, University of Iowa Carver College of Medicine, Iowa City, IA, USA [2]Department of Ophthalmology and Visual Sciences, University of Iowa Carver College of Medicine, Iowa City, IA, USA [3]Department of Molecular Physiology and Biophysics, University of Iowa Carver College of Medicine, Iowa City, IA, USA [4]Metabolomics Core Facility, Carver College of Medicine, University of Iowa, Iowa City, IA, USA [5]Department of Internal Medicine, University of Iowa Carver College of Medicine, Iowa City, IA, USA [6]Fraternal Order of Eagles Diabetes Research Center, University of Iowa Carver College of Medicine, Iowa City, IA, USA [7]Obesity Research and Educational Initiative, University of Iowa Carver College of Medicine, Iowa City, IA, USA [8]Iowa City VA Health Care System, Iowa City, IA, USA

*Corresponding author. Department of Neuroscience and Pharmacology, University of Iowa Carver College of Medicine, Iowa City, IA, 52242, USA. Fax: +319 353 5350. E-mail: kamal-rahmouni@uiowa.edu (K. Rahmouni).

Received June 3, 2021 • Revision received June 29, 2021 • Accepted July 19, 2021 • Available online 23 July 2021

https://doi.org/10.1016/j.molmet.2021.101308

specific disruption of the BBSome reduces vascular relaxation and enhances the contraction responses, which were associated with an increase in aortic stiffness [17]. We demonstrated that these vascular changes, which occur in a manner independent of alterations in blood pressure and body weight, involve the renin-angiotensin system, indicated by the increase in vascular angiotensinogen gene expression and the ability of losartan, an angiotensin type 1 receptor antagonist, to normalize vascular reactivity in smooth muscle—specific *Bbs1*-deficient mice. However, the contribution of the BBSome in endothelial cells to the regulation of vascular function and related physiological processes remains unknown.

Here, we tested the hypothesis that the BBSome in endothelial cells is implicated in the control of vascular function. Consistent with this hypothesis, we show that endothelial-specific BBSome disruption alters endothelial relaxation, but not that of the smooth muscle. Surprisingly, our data demonstrate that endothelial-specific BBSome deficiency affects body weight, lipid accumulation in the liver, and processes related to retinal function. Our findings establish an important role of the endothelial BBSome in the regulation of vascular tone and related physiological processes, including body weight, liver metabolism, and retinal function.

2. MATERIAL AND METHODS

2.1. Animals

To selectively disrupt the BBSome in endothelial cells, we crossed $Bbs1^{fl/fl}$ female mice with $Tie2^{Cre}$ male mice, in which Cre recombinase is driven by a pan-endothelial-specific Tie2 promoter [18] (Strain: B6.Cg-Tg (Tek-cre)1Ywa/J; The Jackson Laboratory, stock no. 008863). To visualize Cre recombinase, we first crossed the $Tie2^{Cre}$ mice with the ROSA (tdTomato) reporter transgenic mouse line, in which a stop codon flanked by loxP sites precedes the start position of a tdTomato locus (Strain: ROSA [$Stop^{fl/fl}$-tdTomato]; The Jackson Laboratory, stock no. 007914). Cre recombination removes the stop site, leading to the expression of the fluorescent tdTomato protein. All mice were maintained on the C57BL/6 J background for this study. The age at which mice were studied is indicated in the description of the results of each experiment.

Genotyping of the mice was performed using a polymerase chain reaction (PCR) assay, as described previously [4]. Animals were housed at the University of Iowa vivarium in a 23 °C temperature-controlled environment with a 12-h:12-h light—dark cycle (lights on: 6 AM—6 PM), with ad libitum access to tap water and either standard chow or a high-fat/high-sucrose (HFHS) diet (Research Diets Inc, D12331). Animal procedures were approved by the University of Iowa Institutional Animal Care and Use Committee.

2.2. Radiotelemetry measurements

Arterial pressure, heart rate, and locomotor activity were recorded continuously using radiotelemetry probes (PA-C10, Data Science Instruments) as described previously [16,17]. Under isoflurane anesthesia and aseptic surgical conditions, the catheter of the telemeter was inserted into the left carotid artery and tied securely using 6-0 silk suture. The transmitter was tunneled subcutaneously from the neck to the midabdominal region. The neck incision was sutured with 4-0 absorbable cat gut and further sealed with tissue adhesive (VetBond) along the incision line. Animals recovered for at least 10 days before recording continued in the conscious unrestrained state. Blood pressure, heart rate, and locomotor activity were recorded for 10 s every 5 min using Data Science Dataquest software.

2.3. Body weight and food intake

Body weight and food intake were measured in the home cages of singly housed mice. Mice were weighed once weekly from 6 to 16 weeks of age. Body composition (fat and lean masses) was determined by nuclear magnetic resonance using a Bruker Minispec. After singly housed mice acclimated for a week, measurements of 24-h food intake for 5 consecutive days were performed.

2.4. Metabolic cages

A 16-channel Promethion system (Sable Systems International) consisting of environmentally controlled cages was used to measure energy expenditure. Mice were acclimatized for 48 h to the metabolic chambers before a 72-h continuous measurement of energy expenditure was performed.

2.5. Glucose tolerance test (GTT) and insulin tolerance test (ITT)

For the GTT, mice were fasted overnight, and blood obtained from the tail was used to measure glucose at baseline (time 0), then at 15, 30, 60, and 120 min after intraperitoneal injection of D-glucose (1 g/kg; Sigma—Aldrich, Cat. No. G8270). To obtain blood, a 1—2 mm piece of tissue was cut from the tail tip distal to the bone with sharp scissors. The tail was then gently massaged to produce blood (1—2 μL), which was collected directly on a glucose test strip (ONETOUCH Ultra). For the ITT, mice were fasted for 5 h. After baseline glucose levels were measured, mice were treated with intraperitoneal insulin (1 U/kg body weight; Novolin, Novo Nordisk) and blood glucose measured again at 15, 30, 60, and 120 min after injection.

2.6. Vascular function

Vascular reactivity experiments were conducted in a suspended organ bath using wire myograph as previously described [11]. In brief, mice were sacrificed with CO_2 asphyxiation and the thoracic aorta and mesenteric artery were quickly removed and placed in Krebs buffer (118.3 mmol/L NaCl, 4.7 mmol/L KCl, 1.2 mmol/L MgSO4, 1.2 mmol/L KH2PO4, 25.0 mmol/L NaHCO3, 2.5 mmol/L CaCl2, 11.0 mmol/L glucose at pH 7.4). Each vessel was cleaned of connective tissue and adventitia fat and cut into rings (aorta 3 mm length; mesenteric artery 2 mm length), which were then mounted on a wire myograph (DMT, Model 610 M) for measurements of isometric tension in heated (37 °C) Krebs solution. Preload for aortic rings was set at ~0.5 g and starting tension (IC_{90}) was applied to all mesenteric rings [17]. Rings were submaximally contracted with prostaglandin F2α (aorta; PGF2α; ~30—50%) or thromboxane A2 receptor agonist (U46619; mesenteric artery), and cumulative vasodilation response curves to acetylcholine (ACh, 1 nmol/L—100 μmol/L) and sodium nitroprusside (SNP, 1 nmol/L—100 μmol/L) were performed. Dose response to vasoconstrictors, PGF2α (1 μmol/L—10 mmol/L), U46619 (1 nmol-10 μmol/L), and KCl depolarization (100 mmol/L) were also assessed. Data are expressed as percentage of relaxation or fold change of maximal contraction to 100 mmol/L KCl.

2.7. Aortic stiffness

Mouse Doppler (MouseDopplerTM, Indus Instruments) was used to measure pulse wave velocity (PWV), which was used as an index of arterial stiffness. Mice anesthetized with 2% isoflurane were placed in a supine position on a heated platform to maintain core body temperature at 37 °C with the help of a rectal probe. Hair was removed from the abdomen before a 20-MHz probe was used to scan the pressure waveforms at the descending aorta and abdominal aorta above the aortic bifurcation. A continuous electrocardiogram was

obtained through the paws. The electrocardiogram and Doppler signals were recorded simultaneously for several cardiac cycles, and the data stored for subsequent analysis. The distance between the descending and abdominal aorta was measured using a caliper. PWV (m/s) was calculated as distance (m) divided by time (s).

2.8. Electroretinogram (ERG)

ERG was used to analyze retinal function [19]. Full-field ERG was performed using the Espion V5 Diagnosys system (Diagnosys LLC, Lowell). The mice were dark-adapted overnight before ERG was conducted. Mice were anesthetized with a mixture of ketamine (87.5 mg/kg) and xylazine (2.5 mg/kg), receiving 0.1 mL of the mixture per 20 g body weight. After the pupils were dilated with 1% tropicamide, ERGs were recorded simultaneously from the corneal surface of each eye using gold ring electrodes (Diagnosys) referenced to a needle electrode (Roland Consult; LKC Technologies Inc.) placed on the back of the head. Gonak gel (Akron, Inc.) was applied to the cornea of each eye before the gold ring electrode was positioned. A second needle electrode placed near the base of the tail served as the ground. Stimuli were presented in a ColorDome (Diagnosys) Ganzfeld bowl, with a camera monitoring mouse head and electrode positions. Dim red light was used for room illumination until dark-adapted testing was completed. A modified International Society for Clinical Electrophysiology of Vision (ISCEV) protocol was used. A dim flash at 0.01 cd s m^{-2} was used first to measure rods, followed by a bright flash at 3.0 cd s m^{-2} to measure the combined standard response (SCR) of the rods and cones. Mice were then light-adapted for 10 min, after which they were tested with a bright flash at 3.0 cd s m^{-2} followed by a flicker of 5 Hz. Evaluation of the ERGs was carried out using MATLAB analysis software.

2.9. Spectral domain optical coherence tomography (OCT) imaging and analysis

OCT is a non-invasive technique for the acquisition of cross-sectional images of retinal structures, from which estimates of the thickness of retinal layers can be made [19,20]. To measure OCT, mice were anesthetized with a mixture of ketamine (87.5 mg/kg) and xylazine (12.5 mg/kg) by intraperitoneal injection and corneas were kept lubricated with Balanced Salt Solution (BSS®; Alcon Laboratories). Anesthetized mice were placed onto an adjustable cassette connected to a platform that allows three-dimensional movement (Bioptigen Envisu R2200). OCT scanning was centered on the optic nerve head of the retina and aligned with the horizontal and vertical planes [20]. OCT volume dimensions were 1000 × 100 × 1024 voxels (1.4 × 1.4 × 1.566 mm^3). Following imaging, mice were administered Atipamezole (0.20 mg/kg of body weight; Antisedan® Injection) and provided supplemental indirect warmth for anesthesia recovery, and their eyes were hydrated with ointment (Artificial Tears, Akorn) as described previously [21].

All OCT scans were analyzed manually with the Bioptigen InVivoVue software. Measurements of the structural thickness of the retinas were collected from three groups of layers and are defined as follows: total retinal thickness was measured from the nerve fiber layer (NFL) to the retinal pigment epithelium (RPE), inner retinal thickness was measured from the NFL to internal limiting membrane (ILM), and outer retinal thickness was measured from the external limiting membrane (ELM) to the RPE. Measurements from two regions of interest on each side of the parafoveal region were collected and averaged for each individual retina.

2.10. Endothelial cell sorting

Endothelial cells were isolated from fresh kidneys that were extracted and digested in an endothelial cell digestion buffer: MCDB-131 complete media, collagenase A (1 mg/mL), collagenase B (1 mg/mL), and DNase1 (100 μg/mL) at 37 °C for 20 min. Cell suspension was subjected to cell sorting using the neonatal cardiac endothelial cell isolation kit (130-104-183, Miltenyi Biotec) and autoMACS Magnetic Cell Separator of Miltenyi according to the manufacturer's instructions.

2.11. Liver histology and immunohistochemistry

For hematoxylin and eosin (H&E) staining, fresh livers were obtained from animals sacrificed with CO_2 and immediately placed in 10% formalin overnight. The tissue was paraffin-embedded and then sectioned at 5 μm. Standard H&E staining procedures were performed by the Central Microscopy Research Facility of the University of Iowa. For staining of neutral lipids, the standard Oil Red O procedure was used. Briefly, fresh liver tissue was dehydrated in 30% sucrose solution for 1 h and then quickly frozen in a dry ice and isopropanol bath. Tissues were subsequently embedded in an optimal cutting temperature fixation medium. Frozen liver tissue was cryosectioned at 10 μm; sections were then incubated in filtered Oil Red O solution (O0625, Sigma—Aldrich) for 7 min and washed with running tap water for 10 min. Water—soluble medium (Vector Laboratories) was used for coverslip mounting. Liver sections were stained by standard H&E or Masson trichrome protocol for general tissue architecture as well as collagen staining (Central Microscopy Research Facility, University of Iowa). Images were obtained using a light microscope (Leica DMi1, Olympus) and quantified using Fiji/ImageJ (National Institutes of Health).

2.12. Serum lipid and enzyme measurements

One hundred μL of plasma was used to determine the lipid profile and alanine aminotransferase (ALT) and aspartate aminotransferase (AST) levels using the Piccolo Lipid Panel Plus (Abaxis, Inc.).

2.13. Metabolomic assays

Liver samples (40 mg) obtained from non-fasted mice were lyophilized overnight prior to extraction. Samples were homogenized in the extraction buffer (720 μL ice cold 2:2:1 methanol/acetonitrile/water which contained a mixture of 9 internal standards (d4-Citric Acid, 13C5-Glutamine, 13C5-Glutamic Acid, 13C6-Lysine, 13C5-Methionine, 13C3-Serine, d4-Succinic Acid, 13C11-Tryptophan, d8-Valine; Cambridge Isotope Laboratories) at a concentration of 1 μg/mL each) using a ceramic-bead mill homogenizer. Liver homogenates were then incubated at −20 °C for 1 h before centrifugation at 4 °C for 10 min at 21,000×*g*. 150 μL (for gas chromatography—mass spectrometry [GC—MS]) or 400 μL (for liquid chromatography—mass spectrometry [LC-MS]) of the cleared metabolite extracts were transferred to fresh tubes for additional processing. An equal volume of each cleared extract was pooled and served as a quality control (QC) sample, which was analyzed at the beginning, end, and at a regular interval throughout an instrument run. The extraction buffer alone was analyzed as a processing blank sample. Metabolite extracts, the QC sample, and the processing blank were evaporated to dryness using a speed-vac.

For GC—MS, the resulting dried metabolite extracts, QC sample, and processing blank sample were derivatized using methyoxyamine hydrochloride (MOX) and N,O-Bis(trimethylsilyl)trifluoroacetamide (TMS) (Sigma). Briefly, dried extracts were reconstituted in 30 μL of 11.4 mg/mL MOX in anhydrous pyridine (VWR), vortexed for 10 min, and heated at 60 °C for 1 h. Next, 20 μL TMS was added to each reconstituted extract, vortexed for 1 min, and heated at 60 °C for 30 min. The derivatized metabolite extracts, blanks, and QC were immediately analyzed using GC—MS.

Gas chromatographic separation was conducted on a Thermo Trace 1300 GC with a TraceGold TG-5SilMS column (0.25 μm film thickness; 0.25 mm ID; 30 m length). An injection volume of 1 μL was used for all samples, blanks, and QCs. The GC was operated in split mode with the following settings: 20:1 split ratio, split flow: 24 μL/min, purge flow: 5 mL/min, carrier mode: constant flow, carrier flow rate: 1.2 mL/min. The GC inlet temperature was 250 °C. The GC oven temperature gradient was as follows: 80 °C for 3 min, increased at 20 °C/min to a maximum temperature of 280 °C, which was held for 8 min. The injection syringe was washed 3 times with pyridine between each sample. Metabolites were detected using a Thermo ISQ single quadrupole mass spectrometer. The data were acquired from 3.90 to 21.00 min in EI mode (70eV) by single ion monitoring (SIM).

For LC-MS, the resulting dried metabolite extracts, QC sample, and processing blank sample were reconstituted in 40 μL of acetonitrile/water (1:1, V/V), vortexed, centrifuged at 4 °C for 10 min at 21,000×*g*, and transferred to autosampler vials for analysis.

Two μL of reconstituted metabolite extracts, QC sample, and processing blank were separated using a Millipore SeQuant ZIC-pHILIC column (2.1 × 150 mm, 5 μm particle size) with a ZIC-pHILIC guard column (20 × 2.1 mm) attached to a Thermo Vanquish Flex UHPLC. The mobile phase was comprised of Buffer A: 20 mM (NH4) 2CO3, 0.1% NH4OH and Buffer B: acetonitrile. The chromatographic gradient was run at a flow rate of 0.150 mL/min as follows: 0—21 min—linear gradient from 80% to 20% Buffer B; 20—20.5 min—-linear gradient from 20% to 80% Buffer B; and 20.5—28 min—hold at 80% Buffer B [20]. Data were acquired using a Thermo Q Exactive MS operated in full-scan, polarity-switching mode with a spray voltage set to 3.0 kV, the heated capillary held at 275 °C, and the HESI probe held at 350 °C. The sheath gas flow was set to 40 units, the auxiliary gas flow to 15 units, and the sweep gas flow to 1 unit. MS data acquisition was performed in a range of 70—1000 *m/z* with the resolution set at 70,000, the AGC target at 10e6, and the maximum injection time at 200 ms.

For GC- and LC-MS, TraceFinder 4.1 was utilized to identify metabolites based on *m/z* and retention time information corresponding to that of a validated in-house library with analysis of authentic standards. After metabolite identification and peak area integration by TraceFinder, the NOREVA tool was used for signal drift correction on a metabolite-to-metabolite basis using multiple analyses of the QC sample throughout the instrument run [22]. Two normalization methods were applied: (1) total ion signal and (2) normalization to weight. Metabolomics data were further analyzed using MetaboAnalyst (http://www.metaboanalyst.ca).

2.14. Quantitative real-time PCR

Total RNA was isolated from each tissue (aorta, mesenteric artery, and liver) using a column-based purification RNA kit (Qiagen). mRNAs were reverse transcribed using an iScript cDNA synthesis kit (Bio-Rad). Quantitative PCR was performed using an iQ5 real-time PCR machine (Bio-Rad) and iScript SYBR green master mix (Bio-Rad). Primer sequences used in this study are provided in the supplemental table. Data were normalized to 18 S (internal control) and expressed as fold change normalized to control.

2.15. Western blotting

Vascular proteins were isolated through homogenization in a lysis buffer containing the following: 50 mmol/L Tris-Cl pH7.5, 0.1 mmol/L ethylenediaminetetraacetic acid, 0.1 mmol/L ethylene glycol-bis (β-aminoethyl ether), 1 mmol/L phenylmethylsulfonyl fluoride, 1 mmol/L NaVO4, 10 mmol/L NaF, 1 mmol/L sodium pyrophosphate, 0.001% sodium deoxycholic acid (W/V), 1% Tergitol-type (NP)-40 (V/V), 0.1% SDS (W/V), and a protease inhibitor cocktail tablet (Roche). Proteins were then subjected to SDS-PAGE and transferred to polyvinylidene fluoride membranes. Membranes were blocked with 5% nonfat dry milk, then incubated with primary antibodies for phosphorylated endothelial nitric oxide synthase (eNOS; 1:1000; Cell Signaling #9571; BD Biosciences #612393), total eNOS (1:1000; BD Biosciences #610297), or β-actin (1:50 000; Proteintech #60008). Proteins were detected using anti-rabbit (1:10 000; Cell Signaling #7074) or anti-mouse horseradish peroxidase (1:10 000; Cell Signaling #7076) conjugated secondary antibodies. Protein expression was visualized by an ECL Prime chemiluminescent detection kit (GE Healthcare) on film, and densitometry (arbitrary units) was calculated using ImageJ.

2.16. Dihydroethidium (DHE) staining

Reactive oxygen species (ROS) production in aorta was evaluated using DHE staining (Sigma). Fresh aortic rings were embedded in the Tissue-Tek optimal cutting temperature compound and sectioned at 10 μm. Sections were then fixed with 4% paraformaldehyde for 20 min at room temperature before being incubated for 30 min at 37 °C in phosphate-buffered saline (PBS) (1 ×) containing 8 μmol/L dihydroethidium. Sections were then washed 3 times with 1 × PBS and mounted with VectaShield mounting medium with 4′,6-diamidino-2-phenylindole. Dihydroethidium images were visualized with confocal microscopy (Zeiss LSM710) at an excitation/emission of 488/568 nm. Three images were taken per sample, each quantified by measuring the mean fluorescent intensity (Zeiss Zen software).

2.17. Statistical analysis

Results are shown as means ± SEM. Data were analyzed using Student's t-test or one- or two-way analysis of variance (ANOVA) with or without repeated measures. When ANOVA reached significance, a post hoc comparison was made using Fisher's test. A $P < 0.05$ was considered statistically significant.

3. RESULTS

3.1. *Bbs1* gene deletion in vascular endothelial cells

To understand the role of the BBSome in endothelial cells, we generated a mouse model lacking the *Bbs1* gene specifically in endothelial cells by crossing $Bbs1^{fl/fl}$ mice with $Tie2^{Cre}$ mice. First, we confirmed the specificity of $Tie2^{Cre}$ expression in the endothelial cell layer by breeding $Tie2^{Cre}$ mice with a tdTomato reporter mouse model. The red fluorescence of tdTomato was observed in the endothelial layer of tdTomato/$Tie2^{Cre}$ mice, but not in other layers, such as the smooth muscle cells of the aorta (Figure 1A). In addition, tdTomato co-localized with the endothelial marker, CD31 (Figure 1B). To confirm endothelial deletion of the *Bbs1* gene, we measured *Bbs1* gene expression in endothelial cells isolated from $Bbs1^{fl/fl}$/$Tie2^{Cre}$ mice (referred to in the figures as $Bbs1^{fl/fl}$/$Tie2^{Cre+}$) and controls ($Bbs1^{fl/fl}$/$Tie2^{Cre-}$). As expected, Bbs1 mRNA levels were significantly decreased in the conditional null mice compared to the controls (Figure 1C). However, there was no change in *Bbs1* gene expression in the liver of $Bbs1^{fl/fl}$/$Tie2^{Cre}$ mice (Supplemental Figure 1), further supporting the specificity of *Bbs1* gene deletion to the endothelium.

3.2. Vascular effects of endothelial *Bbs1* gene deletion

To determine whether loss of the *Bbs1* gene in endothelial cells affects vascular function, we assessed the vascular reactivity to various vasoactive agents of aortic and mesenteric rings of 14- to 16-week-old mice. Interestingly, we found that endothelial *Bbs1* gene deletion

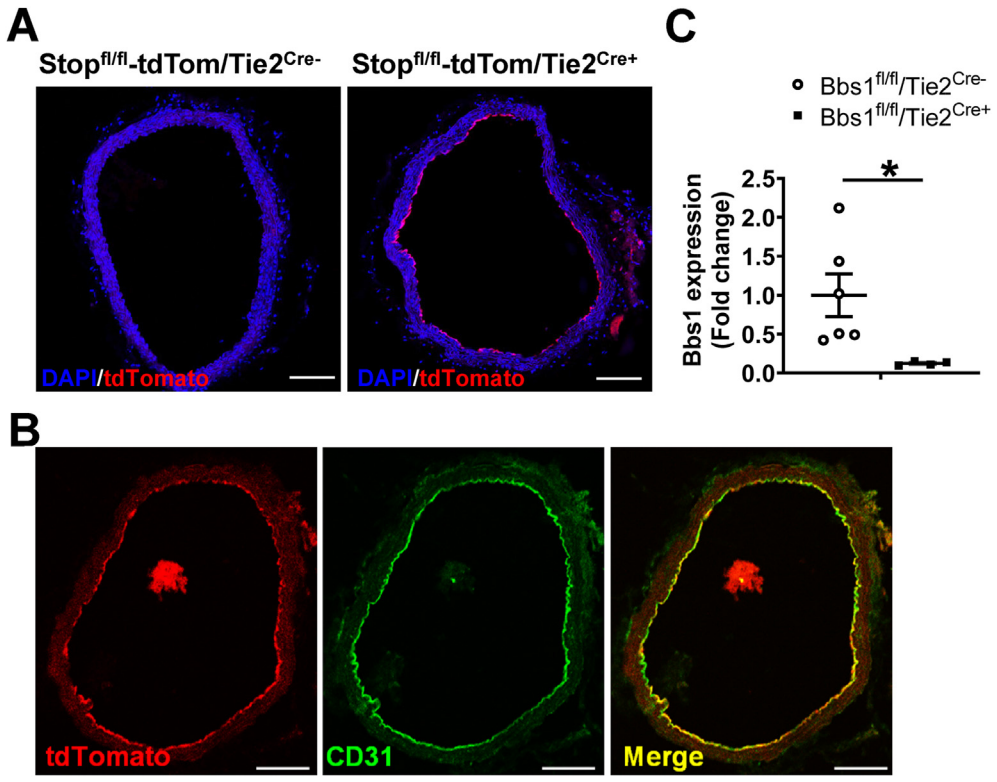

Figure 1: Validation of endothelial-specific *Bbs1* gene knockout mice. (A) Evidence of endothelial-specific Cre recombinase (presence of red fluorescent tdTomato) in the aorta of Stop$^{fl/fl}$-tdTomato/Tie2^{Cre} reporter mice (Stop$^{fl/fl}$-tdTomato/Tie2^{Cre+}), but not controls (Stop$^{fl/fl}$-tdTomato/Tie2^{Cre-}). (B) Co-localization of tdTomato with the endothelial marker CD31 in Stop$^{fl/fl}$-tdTomato/Tie2^{Cre} + mice. (C) Reduction in Bbs1 mRNA levels in magnetically sorted endothelial cells of Bbs1$^{fl/fl}$/Tie2^{Cre} + mice relative to littermate controls (Bbs1$^{fl/fl}$/Tie2^{Cre-}). *$P < 0.05$ by unpaired t-test. Scale bar: 100 μm. (For interpretation of the references to color in this figure legend, the reader is referred to the Web version of this article.)

impaired the endothelium-dependent vasorelaxation evoked by acetylcholine in the aorta and mesenteric artery in mice of both sexes (Figure 2A–D). Of note, the impaired vasorelaxation was more pronounced in female (Figure 2B,D) than male Bbs1$^{fl/fl}$/Tie2^{Cre} mice (Figure 2A,C). Moreover, the endothelial dysfunction was more evident in the mesenteric artery (Figure 2C–D) than in the aorta (Figure 2A–B). On the other hand, the endothelium-independent vasorelaxation responses induced by sodium nitroprusside were intact (Supplemental Figures 2A–D), suggesting that endothelial BBSome deficiency alters the endothelial, but not smooth muscle, vasorelaxation responses.

We next asked whether endothelial-specific *Bbs1* gene deletion affects the ability of the aorta and mesenteric artery to contract in response to various stimuli. Maximal depolarization to KCl (100 mmol/L) tended to be elevated in the mesenteric artery of male Bbs1$^{fl/fl}$/Tie2^{Cre} mice compared to controls (Figure 2G–H), but not in the aorta (Figure 2E–F). Moreover, the response induced by thromboxane A2 receptor agonist (U46619) was significantly increased in the mesenteric rings of male Bbs1$^{fl/fl}$/Tie2^{Cre} mice, specifically (Figure 2K–L). However, there was no difference in the contractile response of the aorta to PGF2α (Figure 2I–J). These data indicate gender- and vascular bed–specific alterations in the contractile responses evoked by endothelial cell–specific *Bbs1* gene deletion.

3.3. Endothelial *Bbs1* gene deletion increases angiotensinogen gene expression

The reduced acetylcholine responses in Bbs1$^{fl/fl}$/Tie2^{Cre} mice point to a potential alteration in NO. However, the expression ratio of phospho-eNOS (Ser1177) to total eNOS protein was unchanged in the aorta and mesenteric artery of Bbs1$^{fl/fl}$/Tie2^{Cre} mice (Figure 3A). Reactive oxygen species (ROS) generation assessed using dihydroethidium (DHE) staining was also not different in the aorta of Bbs1$^{fl/fl}$/Tie2^{Cre} mice relative to controls (Figure 3B).

Given our previous work implicating overactivation of the renin-angiotensin system caused by an increase in angiotensinogen gene expression in the vascular dysfunction evoked by smooth muscle cell *Bbs1* gene deletion [17], we chose to compare angiotensinogen gene expression between Bbs1$^{fl/fl}$/Tie2^{Cre} and control mice. We found a significant ($P < 0.05$) increase in angiotensinogen mRNA levels in the aorta and mesenteric artery of female Bbs1$^{fl/fl}$/Tie2^{Cre} mice (Figure 3C). Angiotensinogen mRNA levels also tended to be higher in the aorta and mesenteric artery of male Bbs1$^{fl/fl}$/Tie2^{Cre} mice relative to controls without reaching statistical significance (Figure 3D). Thus, the activation of the renin-angiotensin system may explain the impaired endothelial function in mice lacking the *Bbs1* gene in endothelial cells.

3.4. Effects of endothelial *Bbs1* gene deletion on blood pressure and arterial stiffness

To determine whether the vascular changes associated with endothelial *Bbs1* gene deletion translate into changes in the hemodynamic parameters, we used radiotelemetry to measure blood pressure and heart rate in 14- to 17-week-old mice. However, there was no difference in systolic, diastolic, or mean arterial pressure between Bbs1$^{fl/fl}$/Tie2^{Cre} mice and controls (Supplemental Figures 3A–B and 3E–F). Interestingly, heart rate was increased selectively in male Bbs1$^{fl/fl}$/

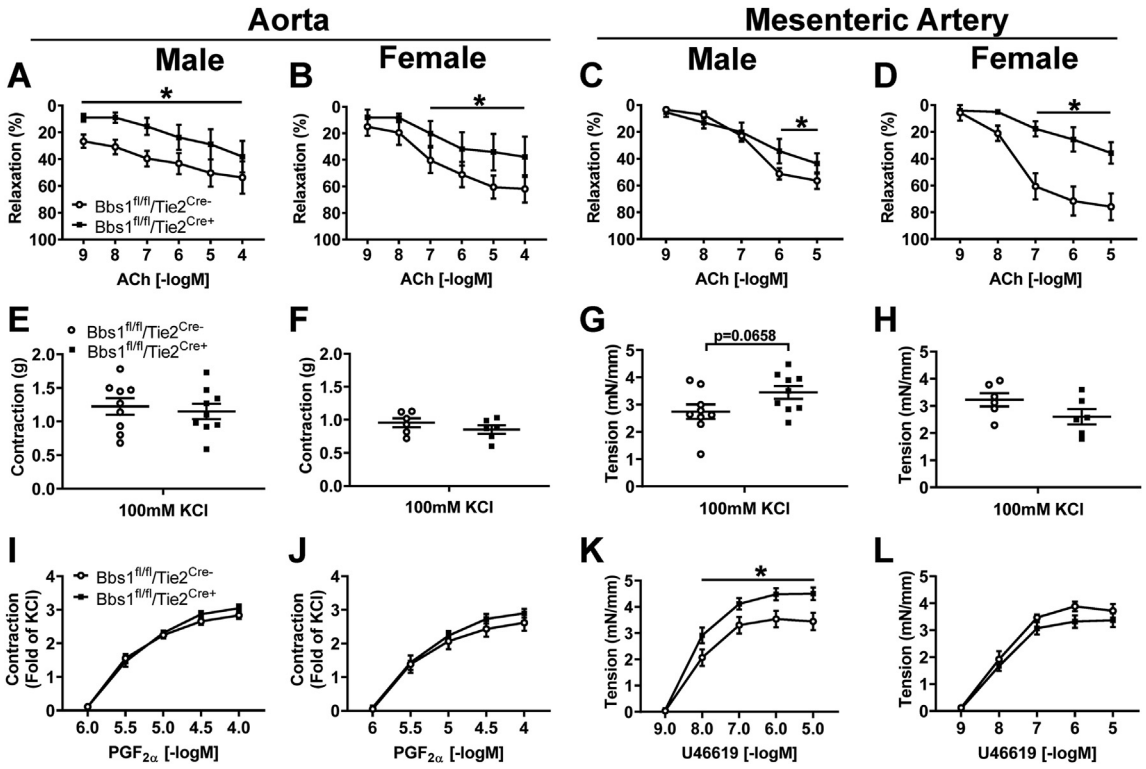

Figure 2: Vascular effects of endothelial-specific *Bbs1* gene deletion. Relaxation responses induced by acetylcholine (ACh; A—D) and contractile responses evoked by KCl (E—H), prostaglandin F2α (PGF2α; I and J), and thromboxane A2 receptor agonist (U46619, K and L) in aortic and mesenteric arterial rings of male and female Bbs1$^{fl/fl}$/Tie2^{Cre+} mice and controls (Bbs1$^{fl/fl}$/Tie2^{Cre-}) fed normal chow. Male: n = 9/group, female: n = 6/group. *P < 0.05 by two-way ANOVA with repeated measure (A—D and I—L) or unpaired t-test (E—H).

Tie2^{Cre} mice during the light cycle (Supplemental Figures 3C and 3G). Locomotor activity was not affected by endothelial *Bbs1* gene deletion (Supplemental Figures 3D and 3H). Based on pulse wave velocity measurements, there was also no difference in arterial stiffness between Bbs1$^{fl/fl}$/Tie2^{Cre} mice and controls (Supplemental Figures 4A—B). These data indicate that the vascular dysfunction evoked by endothelial cell-specific *Bbs1* gene deletion alters daytime heart rate but does not affect blood pressure or arterial stiffness.

3.5. Influence of endothelial *Bbs1* gene on body weight and glucose homeostasis

Endothelial cells play a pivotal role in metabolic regulation, which means endothelial dysfunction can contribute to metabolic disorders like obesity and type 2 diabetes, conditions that are prevalent in BBS [22—24]. Thus, we examined the effects of endothelial *Bbs1* gene deletion on body weight and energy balance. Interestingly, male Bbs1$^{fl/fl}$/Tie2^{Cre} mice displayed increased body weight that was statistically significant at 15—16 weeks of age (Figure 4A). Fat mass tended to be higher in the male Bbs1$^{fl/fl}$/Tie2^{Cre} mice (Figure 4B). On the other hand, female Bbs1$^{fl/fl}$/Tie2^{Cre} mice exhibited a slight (but not statistically significant) increase in body weight that was associated with significantly more body fat without change in lean mass (Figure 4C—D). However, food intake and energy expenditure of 17- to 20-week-old male and female Bbs1$^{fl/fl}$/Tie2^{Cre} mice were not altered relative to control animals (Supplemental Figures 5A—D). To determine whether loss of the endothelial *Bbs1* gene sensitizes mice to diet-induced obesity, we challenged Bbs1$^{fl/fl}$/Tie2^{Cre} mice with a high-fat/high-sucrose (HFHS) diet. Notably, the HFHS diet revealed enhanced sensitivity of male (but not female) Bbs1$^{fl/fl}$/Tie2^{Cre} mice to weight gain (Figure 4E,G). Fat mass tended to be higher in male Bbs1$^{fl/fl}$/Tie2^{Cre} mice fed the HFHS diet, but lean mass was unchanged (Figure 4F—H). Next, we addressed the effects of endothelial *Bbs1* gene deletion on glucose homeostasis and insulin sensitivity using the glucose tolerance test (GTT) and insulin tolerance test (ITT). Compared to controls, 17-week-old male Bbs1$^{fl/fl}$/Tie2^{Cre} mice displayed similar fasting blood glucose levels at baseline and during GTT (Supplemental Figures 6A—B), but had increased glucose levels at the end of ITT (Supplemental Figures 6C—D). Female Bbs1$^{fl/fl}$/Tie2^{Cre} mice showed no alterations in baseline blood glucose, GTT, and ITT (Supplemental Figures 6E—H). Strikingly, HFHS-fed male Bbs1$^{fl/fl}$/Tie2^{Cre} mice displayed improved GTT (Supplemental Figures 6I—J) despite the increased body weight. Compared to controls, HFHS-fed female Bbs1$^{fl/fl}$/Tie2^{Cre} mice showed similar glucose levels at baseline and during GTT and ITT (Supplemental Figure 6M—P). These results suggest that in male mice, endothelial *Bbs1* gene deletion causes minor impairment in insulin sensitivity in the normal chow-fed condition, but a surprising improvement in glucose tolerance under the HFHS feeding condition. We also assessed vascular function of Bbs1$^{fl/fl}$/Tie2^{Cre} mice fed the HFHS diet. We observed significant impairment in endothelium-dependent vasorelaxation evoked by acetylcholine in aortic (Figure 5A—B) and mesenteric artery rings (Figure 5C—D) in mice lacking the endothelial *Bbs1* gene. However, there was no significant change in the endothelium-independent vasorelaxation induced by SNP, despite a slight (but statistically significant) impairment in the mesenteric artery of the conditional null female mice with a higher dose of SNP (Supplemental Figures 7A—D). The maximal

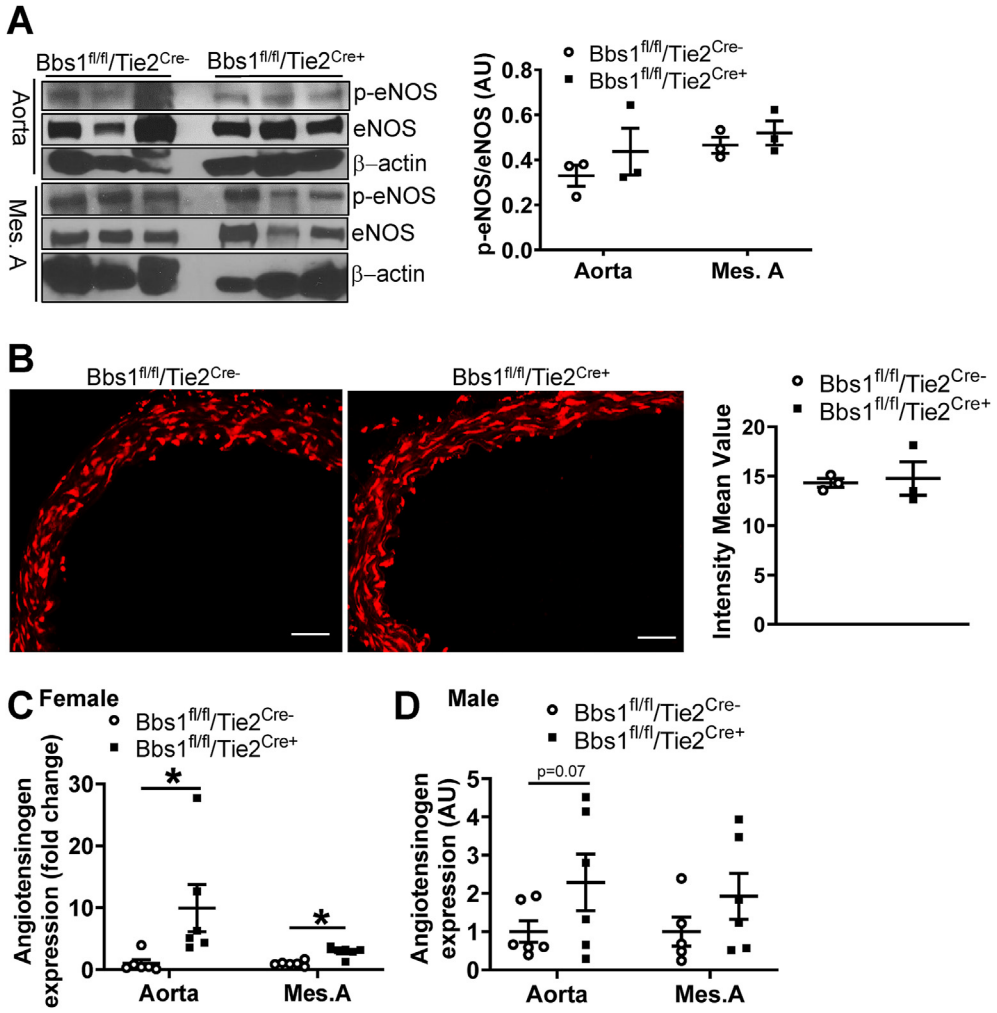

Figure 3: Molecular effects of endothelial-specific *Bbs1* gene deletion in the vasculature. (A) Representative Western blot images and quantification data of phosphorylated (Ser1177) and total endothelial nitric oxide synthase (eNOS) in aortic and mesenteric artery lysates isolated from Bbs1$^{fl/fl}$/Tie2^{Cre+} mice and controls (Bbs1$^{fl/fl}$/Tie2^{Cre-}). β-actin was used as loading control. (B) Representative confocal images of dihydroethidium staining in aorta of control and Bbs1$^{fl/fl}$/Tie2^{Cre+} mice. (C–D) Angiotensinogen mRNA expression in aorta and mesenteric artery of female (C) and male (D) control and Bbs1$^{fl/fl}$/Tie2^{Cre+} mice. *P $<$ 0.05 by Student's t-test. Scale bar: 50 μm.

depolarization to 100 mM KCl was elevated only in the mesenteric artery of male conditional null mice (Figure 5E–H). Additionally, the response to U46619 was slightly (but significantly) reduced at lower concentration in the mesenteric artery of the conditional null female mice fed the HFHS diet (Figure 5I–M).

3.6. Hepatic consequence of endothelial Bbs1 gene deletion

Endothelial dysfunction is thought to be a key event in the development of liver diseases such as steatosis, a disorder that is commonly associated with BBS [25]. Therefore, we examined whether endothelial dysfunction evoked by *Bbs1* gene deletion affects the liver in 32-week-old mice. Based on Masson trichrome and H&E staining, the livers of Bbs1$^{fl/fl}$/Tie2^{Cre} mice exhibited no fibrosis (Supplemental Figure 8A) or architecture alterations (Supplemental Figure 8B). On the other hand, Oil Red O staining revealed increased hepatic lipid content in Bbs1$^{fl/fl}$/Tie2^{Cre} mice that was more pronounced under the HFHS diet (Figure 6A–C). Notably, accumulation of lipid in the livers of Bbs1$^{fl/fl}$/Tie2^{Cre} mice was more profound in females than males (Supplemental Figure 8C).

Measurement of the expression of lipid metabolism–related genes revealed that loss of the endothelial *Bbs1* gene interfered with intracellular or membrane-binding lipid transport processes, as indicated by the significant reduction in the expression of *fatty acid transport protein 1* (*Fatp1*) and *fatty acid binding protein 1* (*FABP1*) as well as the trending increase in the expression of *CD36* and *Fatp5* in male Bbs1$^{fl/fl}$/Tie^{Cre} mice (Figure 6D–E).

We next evaluated how endothelial *Bbs1* gene deletion affects the liver metabolite profile by performing a liver metabolomic analysis of freshly snap-frozen liver tissue. Score plots of selected principal component analysis (PCA) and sparse partial least squares–discriminant analysis (sPLS-DA) showed that Bbs1$^{fl/fl}$/Tie2^{Cre} and control mice belonged to independent liver metabolomics groups (Supplemental Figure 8D–E). Notably, α-ketoglutarate, arachidic acid, guanine, histidine, and tyrosine were elevated in the livers of male Bbs1$^{fl/fl}$/Tie2^{Cre} mice, whereas α-ketoisovalerate and taurine were significantly decreased (Figure 6F–G). In contrast, female Bbs1$^{fl/fl}$/Tie2^{Cre} mice displayed significantly elevated β-alanine, glutamate, guanine, guanosine, and histidine, while hypoxanthine and xanthine tended to be increased (Figure 6F–H). To evaluate

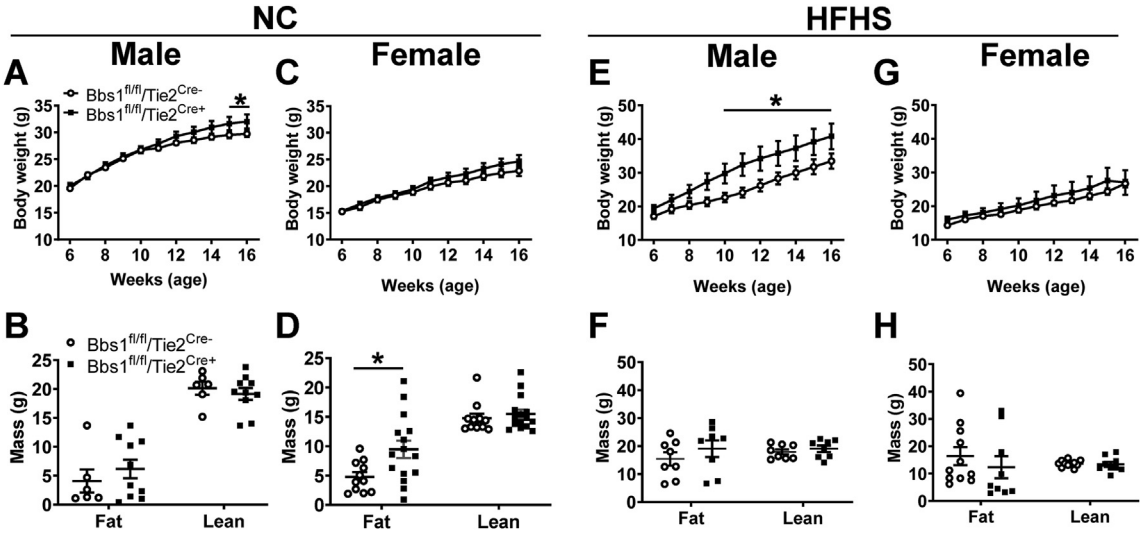

Figure 4: Body weight effect of endothelial-specific *Bbs1* gene deletion. (A–D) Body weight (male: $Bbs1^{fl/fl}/Tie2^{Cre-}$: n = 10 and $Bbs1^{fl/fl}/Tie2^{Cre+}$: n = 11, A; and female: $Bbs1^{fl/fl}/Tie2^{Cre-}$: n = 12 and $Bbs1^{fl/fl}/Tie2^{Cre+}$: n = 17, C) and body composition (B and D) of mice fed normal chow (NC). (E–H) Body weight (male: n = 8/group, E; and female: $Bbs1^{fl/fl}/Tie2^{Cre-}$: n = 11 and $Bbs1^{fl/fl}/Tie2^{Cre+}$: n = 9, G) and body composition (F and H) of mice fed high-fat/high-sucrose (HFHS) diet. *P < 0.05 by two-way ANOVA with repeated measure (body weight) or unpaired t-test (body composition).

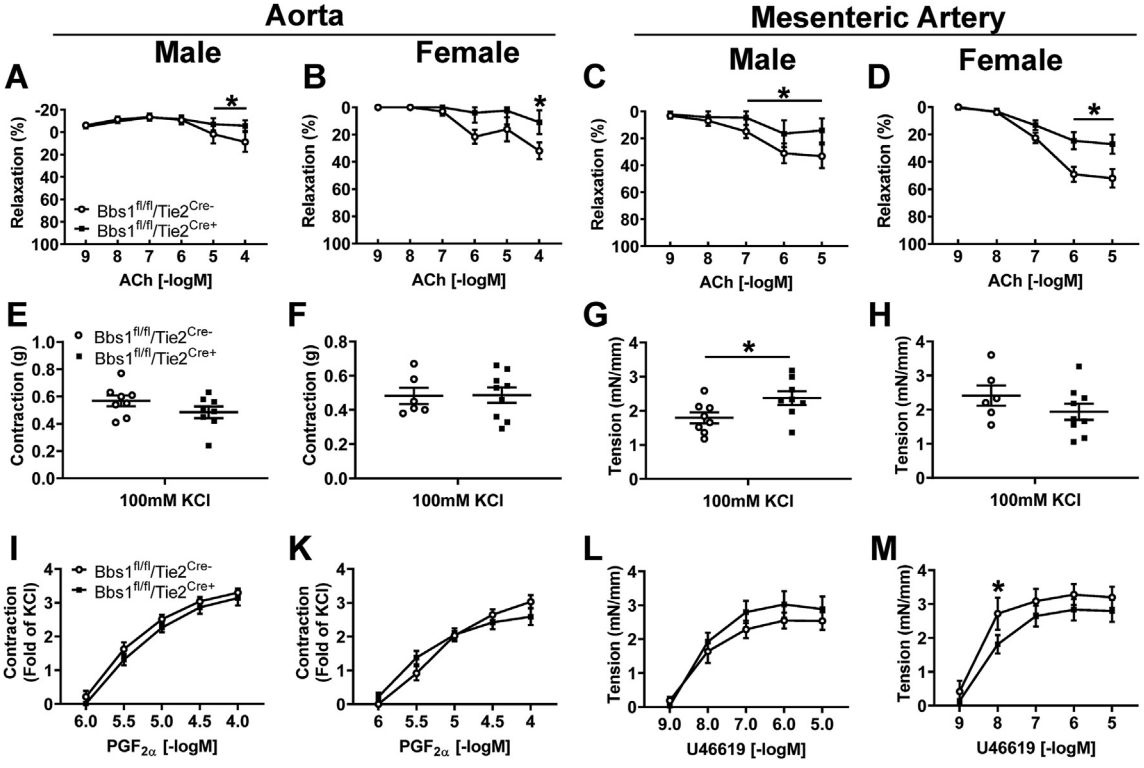

Figure 5: Vascular effects of endothelial-specific *Bbs1* gene deletion under high-fat/high-sucrose (HFHS) diet condition. Relaxation responses induced by acetylcholine (ACh; A–D) and contractile responses evoked by KCl (E–H), prostaglandin F2α (PGF2α; I and J), and thromboxane A2 receptor agonist (U46619; K and L) in aortic and mesenteric arterial rings of male and female $Bbs1^{fl/fl}/Tie2^{Cre+}$ mice and controls ($Bbs1^{fl/fl}/Tie2^{Cre-}$) fed HFHS diet. Male: n = 9/group, female: n = 6/group. *P < 0.05 by two-way ANOVA with repeated measure (A–D and I–L) or unpaired t-test (E–H).

the effect of endothelial *Bbs1* gene deletion on fatty acid metabolites, we performed LC-MS analysis of carnitine metabolites. Female (but not male) $Bbs1^{fl/fl}/Tie2^{Cre}$ mice displayed elevated levels of carnitine (18:1), carnitine (6:0), and trimethylamine n-oxide (Figure 6I–J).

We also evaluated the serum lipid profile and enzyme levels. However, we found no differences in cholesterol, high-density lipoprotein (HDL), triglycerides, and very low-density lipoprotein (VLDL) between $Bbs1^{fl/fl}/Tie2^{Cre}$ mice and controls (Supplemental Figure 7E–F). Liver

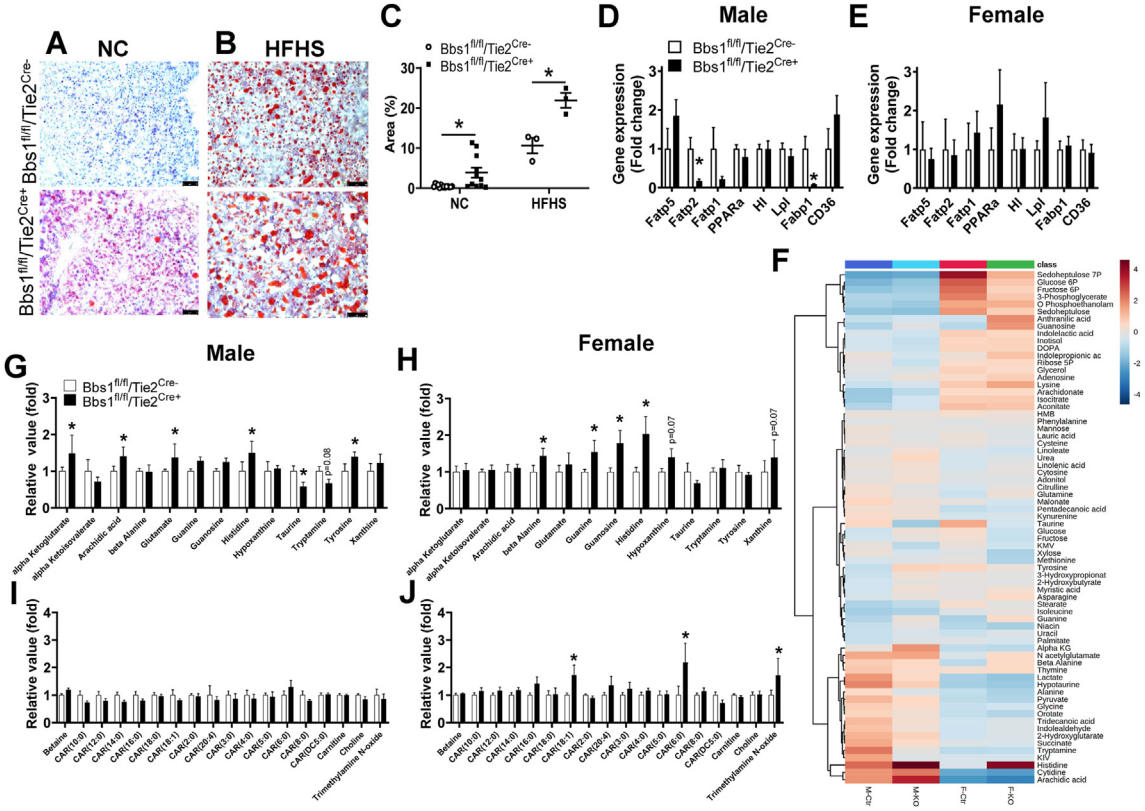

Figure 6: Hepatic effects of endothelial-specific *Bbs1* gene deletion. (A—C) Representative images of hepatic Oil Red O staining in Bbs1$^{fl/fl}$/Tie2^{Cre+} mice and controls (Bbs1$^{fl/fl}$/Tie2^{Cre-}) fed normal chow (NC; A) or high-fat/high-sucrose (HFHS; B) diet and quantitative data (C). The ratio is calculated as the area of pixels that are Oil Red O^{+} relative to total area. (D—E) Expression of genes encoding lipid transport proteins in liver of males (D, n = 6/group) and females (E, n = 3 for controls and n = 5 for Bbs1$^{fl/fl}$/Tie2^{Cre+} mice). (F) Two-way heatmap depicting the GC—MS data. (G—J) Comparison of select metabolites by GC—MS (G and H) and carnitine by LC-MS (I and J) (n = 4—5). *P < 0.01 by unpaired t-test. (For interpretation of the references to color in this figure legend, the reader is referred to the Web version of this article.)

levels of alanine transaminase (ALT) and aspartate transaminase (AST) were also unaffected by endothelial *Bbs1* gene deletion (Supplemental Figure 8F—I).

3.7. Retinal effects of endothelial *Bbs1* gene deletion

Endothelial cells play an essential role in the retina and contribute to the development of various ocular diseases, including those associated with BBS [5,6,26,27]. Thus, we tested whether endothelial *Bbs1* gene deletion affects the retinal function by performing an ERG [19] in 17- to 20-week-old mice. The latency of the b-wave in light-adapted 3.0 bright light stimulation was significantly prolonged in male Bbs1$^{fl/fl}$/Tie2^{Cre} mice without changes in the amplitude (Figure 7B,F). Interestingly, in contrast to males, female Bbs1$^{fl/fl}$/Tie2^{Cre} mice showed significant decrease in amplitude of the a-wave at dark-adapted 3.0 stimulation (Figure 7C), but no difference in b-wave amplitude was noted (Figure 7D). There was no significant alteration in b-wave latency in any condition in female Bbs1$^{fl/fl}$/Tie2^{Cre} mice (Figure 7H). No difference was noted in flicker amplitude in 5 Hz and 30 Hz stimulation between genotypes in either gender (Figure 7I—J).

To test if loss of the *Bbs1* gene in the endothelium affected retinal integrity, we used OCT, a common and useful way of performing quantitative assessments of retinal lamination as well as visualization and localization of exudates, fluid, fibrotic scars, and retinal atrophy [19]. Total retinal thickness was significantly reduced in female Bbs1$^{fl/fl}$/Tie2^{Cre} mice, but not in males (Figure 7K—L). Female Bbs1$^{fl/fl}$/Tie2^{Cre} mice also displayed a trend toward reduction in the inner and outer retinal layers.

4. DISCUSSION

Our study demonstrates the importance of the endothelial BBSome to the regulation of vascular function, with consequences in metabolic control and retinal function. We show that endothelial-specific disruption of the BBSome through *Bbs1* gene deletion causes endothelial dysfunction without affecting smooth muscle vasorelaxation responses. This was associated with enhanced response to contractile agents such as thromboxane A2 receptor agonist (U46619). These vascular changes occurred in a manner independent of blood pressure and arterial stiffness. Surprisingly, endothelial-specific *Bbs1* gene deletion altered adiposity and hepatic lipid content. In addition, mice lacking the *Bbs1* gene in endothelial cells displayed functional and structural changes in the retina. These findings highlight the importance of the endothelial BBSome for the control of various physiological processes.

BBS patients are at high risk of developing cardiovascular disease due to the many risk factors associated with this syndrome [28—30]. Consistent with these observations, BBS proteins and the BBSome have emerged as important regulators of cardiometabolic health, including vascular function. Indeed, we previously demonstrated that loss of the BBSome in smooth muscle cells causes several vascular

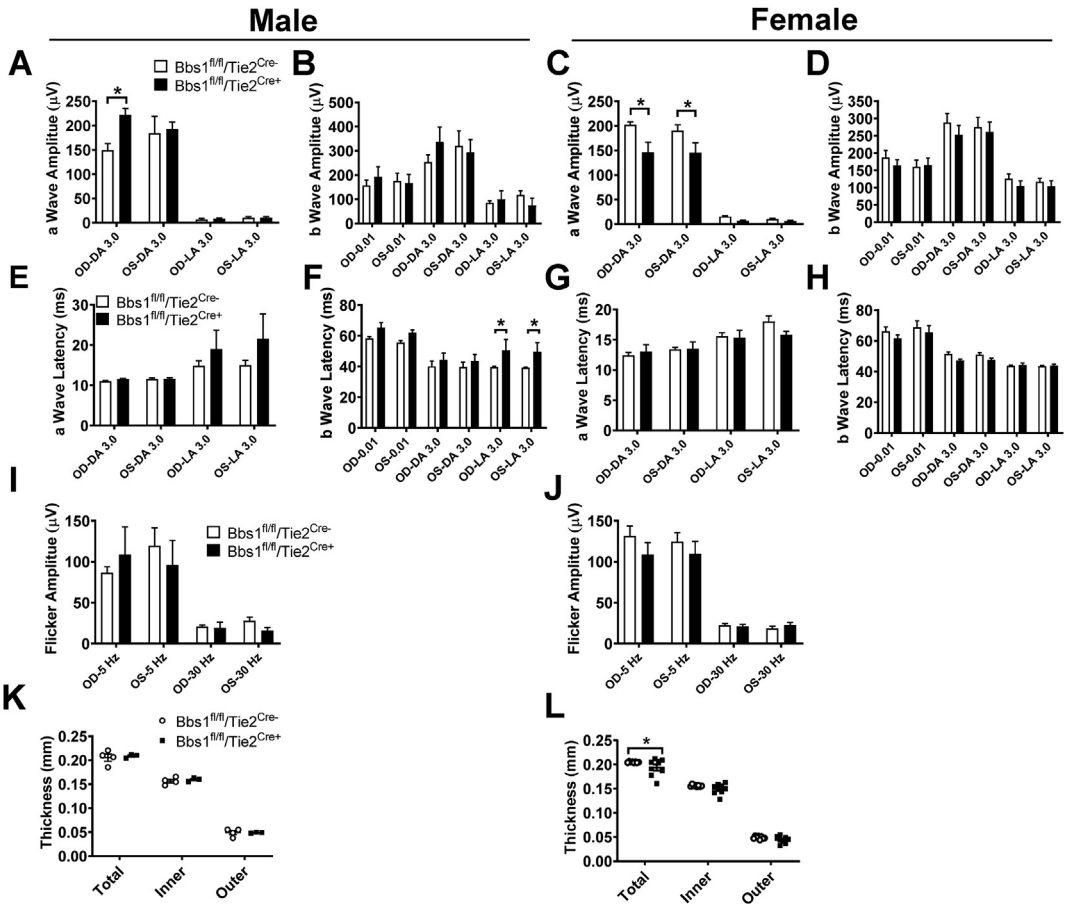

Figure 7: Retinal effects of endothelial-specific *Bbs1* gene deletion. Amplitude (A—D) and latency (E—H) of a- and b-waves and flicker amplitude for 5 Hz and 30 Hz stimulation (I—J) by electroretinogram in males (n = 5 for controls (Bbs1$^{fl/fl}$/Tie2^{Cre-}), n = 4 for Bbs1$^{fl/fl}$/Tie2^{Cre+} mice) and females (n = 7 for controls, n = 8 for Bbs1$^{fl/fl}$/Tie2^{Cre+} mice). (K—L) Thickening of retina by optical coherence tomography in males (n = 8/group) and females (n = 4 for controls, n = 3 for Bbs1$^{fl/fl}$/Tie2^{Cre+} mice). *P < 0.05 by two-way ANOVA.

abnormalities, including reduction in endothelial-dependent and -independent vascular relaxation of the aorta, but not of the mesenteric artery [17]. We also observed an enhanced contractile response to KCl and endothelin-1 in both the aorta and mesenteric artery, whereas the contraction evoked by U46619 was enhanced only in the mesenteric artery of mice lacking the *Bbs1* gene in smooth muscle cells. These vascular changes were associated with increased arterial stiffening without changes in arterial pressure [17]. Our current study points to similarities and differences in the modulation of vascular functions by the BBSome in smooth muscle and the endothelium. Indeed, here we show that endothelial cell—specific BBSome deficiency causes impairment in endothelial but not smooth muscle relaxation in both the aorta and mesenteric artery. This was associated with enhanced contractile response to U46619 in the mesenteric artery of male Bbs1$^{fl/fl}$/Tie2^{Cre} mice without significant alterations in arterial stiffness and blood pressure. Consistent with our previous observations in mice lacking the *Bbs1* gene in smooth muscle cells, our data point to activation of the renin-angiotensin system evoked by elevated angiotensinogen gene expression as a potential mechanism for the vascular changes associated with endothelial *Bbs1* gene deletion. The lack of change in phospho-eNOS and ROS indicates that activation of the renin-angiotensin system contributes to vascular dysfunction independently of these pathways. It should be noted that angiotensin II can alter vascular reactivity through its ability to promote the release and action of norepinephrine, thereby enhancing the neurogenic vasomotor activity [31,32]. Angiotensin II could also contribute to vascular dysfunction by causing T cells and monocytes/macrophages to accumulate in the vasculature [33] or by promoting cell growth and fibrosis [34]. Clearly, further studies are necessary to define the mechanisms by which activation of the renin angiotensin system causes vascular dysfunction in mice lacking the *Bbs1* gene in the endothelium.

Metabolic disorders, including obesity and type 2 diabetes, are among the common features found in BBS patients and mice [35,36]. These metabolic abnormalities are attributed to leptin resistance in the central nervous system and insulin resistance in insulin-sensitive tissues such as adipose tissue and skeletal muscle, caused by disruption of the BBSome [24]. However, our current findings demonstrate the contribution of endothelial cells to the metabolic changes evoked by loss of the BBSome. Indeed, endothelial-specific Bbs1 deletion led to excess weight gain in male mice, an effect that was enhanced with HFHS diet feeding. Our findings are consistent with the notion that vascular endothelial dysfunction is a major driver of metabolic disorders, including excess weight and adiposity [2]. Interestingly, although male *Bbs1* conditional null mice displayed impaired insulin sensitivity under the normal chow diet condition, their glucose tolerance improved under HFHS. The discrepancy between body weight and body composition (more specifically, fat

mass) is also puzzling. For instance, female *Bbs1* conditional null mice fed normal chow display significantly elevated fat mass, but no difference in body weight. It should be noted, however, that although it was not statistically significant, the body weight of female Bbs1$^{fl/fl}$/Tie2^{Cre} mice was ~2 g higher than that of controls, which may explain the increase in fat mass.

The liver endothelium is composed mainly of liver sinusoidal endothelial cells, which are highly specialized endothelial cells that mediate the bidirectional lipid exchange between the blood and the liver parenchyma. Several lines of evidence indicate that endothelial dysfunction plays a major role in the development of hepatic steatosis [37–39]. This is further supported by the presence of hepatic steatosis in Bbs1$^{fl/fl}$/Tie2^{Cre} mice, associated with several changes in the molecular processes relevant to lipid uptake by the liver. Furthermore, analysis of liver metabolites showed that *Bbs1* gene deletion in endothelial cells leads to elevated levels of important hepatic metabolites, including arachidic acid, a 20-carbon saturated fatty acid; the TCA cycle intermediate α-ketoglutarate; the amino acid glutamate, which can be derived from histidine and, in turn, be converted to α-ketoglutarate; glucogenic and ketogenic amino acid tyrosine; β-alanine and histidine that are condensed to form the antioxidant carnosine; guanine, guanosine, hypoxanthine, and xanthine, components of the purine salvage pathway; 18:1 fatty acylcarnitine, an important element in mitochondria fatty acid entry and oxidation; and trimethylamine n-oxide, a carnitine metabolism associated with adverse cardiovascular outcomes. Meanwhile, taurine, a bile salt-forming amino acid derivative, is decreased. These results demonstrate the importance of the endothelial BBSome for overall liver metabolic function in line with fatty acid metabolism. Our results also raise the interesting possibility that dysfunction of the endothelial BBSome may trigger or contribute to hepatic steatosis and non-alcoholic fatty liver disease. However, additional studies are needed to test this possibility.

The endothelium is an important component of the retina, and endothelial dysfunction contributes to ocular diseases and blindness [5,6,26]. In line with this idea, we show that the endothelial dysfunction evoked by loss of the *Bbs1* gene in endothelial cells is associated with several structural and functional abnormalities in the retina, as indicated by the altered ERG and retinal thickness. These findings point to loss of the endothelial BBSome as a potential contributor to or cause of the structural and functional retinal defects associated with BBS. These findings also raise the interesting possibility that dysfunction of the BBSome in endothelial cells may contribute to common forms of retinal diseases such as diabetic retinopathy [27], but this remain to be tested. More work is also needed to understand how disruption of the endothelial BBSome affects retinal structure and function. It is possible that the reduction in the endothelium-mediated vasorelaxation alters the permeability of endothelial cells that disrupt nutritional and oxygen supply. Alternatively, BBSome deficiency may interfere with the inflammatory response or other cellular processes that disturb the electrical function and thickness of the retina.

The differential effect of endothelial BBSome disruption on the various physiological functions in male and female mice point to the sex-specific roles of the endothelial BBSome in the control of these physiological processes. It should be noted that sex differences in phenotypes have also been reported in mice bearing global or neuronal disruption of the BBSome. For instance, obesity is more evident in female than male Bbs knockout mice [36,40]. Interestingly, we found that the increase in vascular angiotensinogen expression was more pronounced in female Bbs1$^{fl/fl}$/Tie2^{Cre} mice, which may explain some of the phenotypes (such as vascular dysfunction) that were more severe in female than male conditional Bbs1 null mice. The dimorphism in the changes in hepatic metabolites and expression of molecules relevant to liver lipid uptake can also explain the sex difference in hepatic steatosis severity. Indeed, the decrease in the expression of Fatps, which mediate long-chain fatty acid update, is consistent with the attenuated hepatic steatosis in male Bbs1$^{fl/fl}$/Tie2^{Cre} mice. On the other hand, the pronounced hepatic steatosis in female Bbs1$^{fl/fl}$/Tie2^{Cre} mice may be driven by the altered hepatic metabolites. However, more studies are required to decipher the mechanisms underlying the sex differences in the expression of vascular angiotensinogen and hepatic molecule and metabolite levels.

One limitation of the present study that is worth mentioning relates to the fact that in addition to endothelial cells, Tie2^{Cre} drives Cre expression in hematopoietic cells [41], which may have contributed to the phenotypes we observed in Bbs1$^{fl/fl}$/Tie2^{Cre} mice. There is also a potential involvement of *Bbs1* gene loss in cell types other than those associated with the phenotypes of Bbs1$^{fl/fl}$/Tie2^{Cre} mice. For instance, in the retina, Tie2^{Cre} signal was previously shown to be present in microglia and macrophage/myeloid cells [42], raising the possibility that *Bbs1* gene deletion in these cells may have contributed to the retinal phenotype of Bbs1$^{fl/fl}$/Tie2^{Cre} mice.

In conclusion, our study demonstrates the importance of the endothelial BBSome for the control of vascular tone and related physiological processes, including energy homeostasis, liver metabolism, and retinal function. Our findings also highlight the significance of the vascular abnormalities for the development of the various diseases associated with BBS.

ACKNOWLEDGMENTS

The authors would like to thank Drs. Brandon Davis and Ling Yang for their input on the studies and Dr. Val Sheffield for providing the Bbs1 conditional mice. We would also like to thank Paul J. Casella for editorial assistance. This work was supported by NIH grant HL084207, VA grant BX004249, and the University of Iowa Fraternal Order of Eagles Diabetes Research Center to KR, T32 to JJ, and 16POST30830004 to JJR. AHB was supported by Training Grant T32 DK112751-01. The contents do not represent the views of the U.S. Department of Veterans Affairs or the U.S. Government.

CONFLICT OF INTEREST

None declared.

APPENDIX A. SUPPLEMENTARY DATA

Supplementary data to this article can be found online at https://doi.org/10.1016/j.molmet.2021.101308.

REFERENCES

[1] Cines, D.B., Pollak, E.S., Buck, C.A., Loscalzo, J., Zimmerman, G.A., McEver, R.P., et al., 1998. Endothelial cells in physiology and in the pathophysiology of vascular disorders. Blood 91(10):3527–3561.

[2] Graupera, M., Claret, M., 2018. Endothelial cells: new players in obesity and related metabolic disorders. Trends in Endocrinology and Metabolism 29(11): 781–794.

[3] Davies, B.S., Beigneux, A.P., Barnes 2nd, R.H., Tu, Y., Gin, P., Weinstein, M.M., et al., 2010. GPIHBP1 is responsible for the entry of lipoprotein lipase into capillaries. Cell Metabolism 12(1):42–52.

[4] Hammoutene, A., Rautou, P.E., 2019. Role of liver sinusoidal endothelial cells in non-alcoholic fatty liver disease. Journal of Hepatology 70(6):1278–1291.

[5] Bharadwaj, A.S., Appukuttan, B., Wilmarth, P.A., Pan, Y., Stempel, A.J., Chipps, T.J., et al., 2013. Role of the retinal vascular endothelial cell in ocular disease. Progress in Retinal and Eye Research 32:102—180.

[6] Resch, H., Garhofer, G., Fuchsjäger-Mayrl, G., Hommer, A., Schmetterer, L., 2009. Endothelial dysfunction in glaucoma. Acta Ophthalmologica 87(1):4—12.

[7] Nachury, M.V., 2018. The molecular machines that traffic signaling receptors into and out of cilia. Current Opinion in Cell Biology 51:124—131.

[8] Datta, P., Allamargot, C., Hudson, J.S., Andersen, E.K., Bhattarai, S., Drack, A.V., et al., 2015. Accumulation of non-outer segment proteins in the outer segment underlies photoreceptor degeneration in Bardet-Biedl syndrome. Proceedings of the National Academy of Sciences of the U S A 112(32):E4400—E4409.

[9] Jin, H., White, S.R., Shida, T., Schulz, S., Aguiar, M., Gygi, S.P., et al., 2010. The conserved Bardet-Biedl syndrome proteins assemble a coat that traffics membrane proteins to cilia. Cell 141(7):1208—1219.

[10] Loktev, A.V., Zhang, Q., Beck, J.S., Searby, C.C., Scheetz, T.E., Bazan, J.F., et al., 2008. A BBSome subunit links ciliogenesis, microtubule stability, and acetylation. Developmental Cell 15(6):854—865.

[11] Nachury, M.V., Loktev, A.V., Zhang, Q., Westlake, C.J., Peränen, J., Merdes, A., et al., 2007. A core complex of BBS proteins cooperates with the GTPase Rab8 to promote ciliary membrane biogenesis. Cell 129(6):1201—1213.

[12] Seo, S., Baye, L.M., Schulz, N.P., Beck, J.S., Zhang, Q., Slusarski, D.C., et al., 2010. BBS6, BBS10, and BBS12 form a complex with CCT/TRiC family chaperonins and mediate BBSome assembly. Proceedings of the National Academy of Sciences of the U S A 107(4):1488—1493.

[13] Seo, S., Zhang, Q., Bugge, K., Breslow, D.K., Searby, C.C., Nachury, M.V., et al., 2011. A novel protein LZTFL1 regulates ciliary trafficking of the BBSome and Smoothened. PLoS Genetics 7(11):e1002358.

[14] Beales, P.L., Elcioglu, N., Woolf, A.S., Parker, D., Flinter, F.A., 1999. New criteria for improved diagnosis of Bardet-Biedl syndrome: results of a population survey. Journal of Medical Genetics 36(6):437—446.

[15] Deveault, C., Billingsley, G., Duncan, J.L., Bin, J., Theal, R., Vincent, A., et al., 2011. BBS genotype-phenotype assessment of a multiethnic patient cohort calls for a revision of the disease definition. Human Mutation 32(6):610—619.

[16] Beyer, A.M., Guo, D.F., Sheffield, V.C., Rahmouni, K., 2010. Contrasting vascular effects caused by loss of Bardet-Biedl syndrome genes. American Journal of Physiology — Heart and Circulatory Physiology 299(6):H1902—H1907.

[17] Reho, J.J., Guo, D.F., Morgan, D.A., Rahmouni, K., 2019. Smooth muscle cell-specific disruption of the BBSome causes vascular dysfunction. Hypertension 74(4):817—825.

[18] Kisanuki, Y.Y., Hammer, R.E., Miyazaki, J., Williams, S.C., Richardson, J.A., Yanagisawa, M., 2001. Tie2-Cre transgenic mice: a new model for endothelial cell-lineage analysis in vivo. Developmental Biology 230(2):230—242.

[19] Seo, S., Mullins, R.F., Dumitrescu, A.V., Bhattarai, S., Gratie, D., Wang, K., et al., 2013. Subretinal gene therapy of mice with Bardet-Biedl syndrome type 1. Investigative Ophthalmology & Visual Science 54(9):6118—6132.

[20] Sohn, E.H., van Dijk, H.W., Jiao, C., Kok, P.H., Jeong, W., Demirkaya, N., et al., 2016. Retinal neurodegeneration may precede microvascular changes characteristic of diabetic retinopathy in diabetes mellitus. Proceedings of the National Academy of Sciences of the U S A 113(19):E2655—E2664.

[21] Koehn, D., Meyer, K.J., Syed, N.A., Anderson, M.G., 2015. Ketamine/xylazine-induced corneal damage in mice. PloS One 10(7):e0132804.

[22] Pi, X., Xie, L., Patterson, C., 2018. Emerging roles of vascular endothelium in metabolic homeostasis. Circulation Research 123(4):477—494.

[23] Starks, R.D., Beyer, A.M., Guo, D.F., Boland, L., Zhang, Q., Sheffield, V.C., et al., 2015. Regulation of insulin receptor trafficking by Bardet Biedl syndrome proteins. PLoS Genetics 11(6):e1005311.

[24] Guo, D.F., Cui, H., Zhang, Q., Morgan, D.A., Thedens, D.R., Nishimura, D., et al., 2016. The BBSome controls energy homeostasis by mediating the transport of the leptin receptor to the plasma membrane. PLoS Genetics 12(2):e1005890.

[25] Branfield Day, L., Quammie, C., Héon, E., Bhan, A., Batmanabane, V., Dai, T., et al., 2016. Liver anomalies as a phenotype parameter of Bardet—Biedl syndrome. Clinical Genetics 89(4):507—509.

[26] Ruan, Y., Jiang, S., Musayeva, A., Gericke, A., 2020. Oxidative stress and vascular dysfunction in the retina: Therapeutic strategies. Antioxidants 9(8):761.

[27] Shin, E.S., Sorenson, C.M., Sheibani, N., 2014. Diabetes and retinal vascular dysfunction. Journal of Ophthalmic and Vision Research 9(3):362—373.

[28] Imhoff, O., Marion, V., Stoetzel, C., Durand, M., Holder, M., Sigaudy, S., et al., 2011. Bardet-Biedl syndrome: a study of the renal and cardiovascular phenotypes in a French cohort. Clinical Journal of the American Society of Nephrology 6(1):22—29.

[29] Forsythe, E., Sparks, K., Hoskins, B.E., Bagkeris, E., McGowan, B.M., Carroll, P.V., et al., 2015. Genetic predictors of cardiovascular morbidity in Bardet-Biedl syndrome. Clinical Genetics 87(4):343—349.

[30] Forsythe, E., Beales, P.L., 2013. Bardet-Biedl syndrome. European Journal of Human Genetics 21(1):8—13.

[31] Balt, J.C., Mathy, M.J., Nap, A., Pfaffendorf, M., van Zwieten, P.A., 2001. Effect of the AT1-receptor antagonists losartan, irbesartan, and telmisartan on angiotensin II-induced facilitation of sympathetic neurotransmission in the rat mesenteric artery. Journal of Cardiovascular Pharmacology 38(1):141—148.

[32] Reardon, T.F., Callaghan, B.P., Brock, J.A., 2015. Angiotensin II increases nerve-evoked contractions in mouse tail artery by a T-type Ca(2+) channel-dependent mechanism. European Journal of Pharmacology 761:11—18.

[33] Itani, H.A., Harrison, D.G., 2015. Memories that last in hypertension. American Journal of Physiology — Renal Physiology 308(11):F1197—F1199.

[34] Ruiz-Ortega, M., Lorenzo, O., Rupérez, M., Esteban, V., Suzuki, Y., Mezzano, S., et al., 2001. Role of the renin-angiotensin system in vascular diseases: expanding the field. Hypertension 38(6):1382—1387.

[35] Green, J.S., Parfrey, P.S., Harnett, J.D., Farid, N.R., Cramer, B.C., Johnson, G., et al., 1989. The cardinal manifestations of Bardet—Biedl syndrome, a form of Laurence—moon—Biedl syndrome. New England Journal of Medicine 321(15):1002—1009.

[36] Davis, R.E., Swiderski, R.E., Rahmouni, K., Nishimura, D.Y., Mullins, R.F., Agassandian, K., et al., 2007. A knockin mouse model of the Bardet-Biedl syndrome 1 M390R mutation has cilia defects, ventriculomegaly, retinopathy, and obesity. Proceedings of the National Academy of Sciences of the U S A 104(49):19422—19427.

[37] Miyao, M., Kotani, H., Ishida, T., Kawai, C., Manabe, S., Abiru, H., et al., 2015. Pivotal role of liver sinusoidal endothelial cells in NAFLD/NASH progression. Laboratory Investigation 95(10):1130—1144.

[38] Sun, X., Harris, E.N., 2020. New aspects of hepatic endothelial cells in physiology and nonalcoholic fatty liver disease. American Journal of Physiology — Cell Physiology 318(6):C1200—C1213.

[39] Furuta, K., Guo, Q., Hirsova, P., Ibrahim, S.H., 2020. Emerging roles of liver sinusoidal endothelial cells in nonalcoholic steatohepatitis. Biology 9(11):395.

[40] Mykytyn, K., Mullins, R.F., Andrews, M., Chiang, A.P., Swiderski, R.E., Yang, B., et al., 2004. Bardet-Biedl syndrome type 4 (BBS4)-null mice implicate Bbs4 in flagella formation but not global cilia assembly. Proceedings of the National Academy of Sciences of the U S A 101(23):8664—8669.

[41] Tang, Y., Harrington, A., Yang, X., Friesel, R.E., Liaw, L., 2010. The contribution of the Tie2+ lineage to primitive and definitive hematopoietic cells. Genesis 48(9):563—567.

[42] Huang, W., Li, Q., Amiry-Moghaddam, M., Hokama, M., Sardi, S.H., Nagao, M., et al., 2016. Critical endothelial regulation by LRP5 during retinal vascular development. PloS One 11(3):e0152833.

